

# Three-body model of ${}^6\text{He}$ with non-local halo effective field theory potentials

E. C. Pinilla,<sup>1,2,3</sup> W. Leidemann,<sup>2,3</sup> G. Orlandini,<sup>2,3</sup> and P. Descouvemont<sup>4</sup>

<sup>1</sup>*Universidad Nacional de Colombia, Sede Bogotá, Facultad de Ciencias,  
Departamento de Física, Grupo de Física Nuclear, Carrera 45 N° 26-85,  
Edificio Uriel Gutiérrez, Bogotá D.C. C.P. 1101, Colombia.*

<sup>2</sup>*Department of Physics, University of Trento, V. Sommarive 14, I-38123 Trento, Italy*

<sup>3</sup>*INFN-TIFPA, V. Sommarive 14, I-38123 Trento, Italy*

<sup>4</sup>*Département de Physique, C.P. 229,  
Université libre de Bruxelles (ULB), B 1050 Brussels, Belgium*

(Dated: September 6, 2024)

We study the  ${}^6\text{He}$  Borromean nucleus in coordinate representation within a three-body model with two-body potentials derived from cluster effective field theory (EFT). These potentials are originally developed in momentum space and Fourier transformed to provide non-local potentials in configuration space. We use hyperspherical coordinates in combination with the Lagrange-mesh technique to compute the ground state energy, root mean square radius and the E1 strength distribution of  ${}^6\text{He}$ . We also introduce a three-body interaction to eliminate dependencies on the cutoff parameter of the two-body potentials on the ground state energy. The E1 strength distribution exhibits a low lying resonance as expected. However it is strongly influenced by the choice of the three-body EFT interaction.

## I. INTRODUCTION

Modern nuclear theory is paying a lot of attention to develop state of the art models as precise as possible to study nuclei. In particular, the derivation of nucleus-nucleus interactions from ab initio theories that allow the prediction rather than the phenomenological explanation of nuclear processes is of current interest.

Effective field theory (EFT) is a powerful framework that takes advantage of the separation of scales in a physical system by integrating out its irrelevant degrees of freedom [1, 2]. In nuclear physics, EFTs have become very popular to study few nucleon configurations (see for instance Refs. [3–6]).

An interesting application of the EFT framework is the study of halo nuclei. Those nuclei can be seen as made up of a core plus one or more nucleons that are weakly bound to the core [7]. Thus, halo nuclei possess a separation of scales: a low momentum scale associated with the weakly bound character of the halo, and a high-momentum scale that corresponds to the binding energy of the core.

A typical example of halo nuclei is  ${}^6\text{He}$ , which can be described as an alpha core plus two weakly bound neutrons forming the halo. This nucleus is called Borromean, since none of the two-body pairs  $\alpha - n$  or  $n - n$  form a bound state. Three-body models with phenomenological local potentials have been widely applied to study the structure and dynamics of this nucleus [8–12].

In Ref. [13], a cluster EFT was used to find the ground state energy of the nucleus  ${}^6\text{He}$ . This is a leading order (LO) three-body halo EFT and assumes that the two-body interactions are dominated by the  $S_0$   $n - n$  and  $P_{3/2}$   $\alpha - n$  partial waves. Other partial waves are regarded as higher-order corrections in their EFT. A three-body EFT interaction was derived at LO to accurately reproduce the  ${}^6\text{He}$  ground state energy and to eliminate cutoff

dependencies. Once the two-body potentials are fixed, the three-body problem is solved using momentum-space Faddeev equations [14].

Cluster EFT potentials are derived in a natural way in momentum space. However, working in this space leads to convergence problems when the Coulomb interaction is present. Thus, a treatment in configuration representation is more convenient, since the Coulomb interaction can be managed in a simpler way. In coordinate space, those potentials become non-local and can be obtained by performing a double Fourier transform.

In principle, the cluster EFT potentials [15–17] are more fundamental than the phenomenological ones, since they are not fitted to reproduce experimental data. Instead, they are derived from the matching to a low-energy theory of the expansion of an observable in a series, up to a chosen order, of the ratio of a typical low-momentum scale, over a high momentum scale. In our case, the low-energy theory is the effective range theory. The low energy constants (LECs) are related to terms of the expansion, which in turn, are related to the effective range parameters. Once, the experimental values of these parameters are inserted, we can get the cluster EFT potentials at some order.

In this work, we employ two-body cluster EFT non-local potentials to study  ${}^6\text{He}$ . We use a three-body model in configuration space with hyperspherical coordinates and the Lagrange mesh technique [18]. In particular, we compute structure properties such as the ground state energy, the root mean square radius (rms), as well as the electric dipole strength distribution. We Fourier transform the cluster EFT  $S$ -wave  $n - n$  potential, and the  $s_{1/2}$  and  $p_{3/2}$   $\alpha - n$  potentials derived in Refs. [15–17] at LO. An  $S$ -wave EFT three-body potential in representation coordinates at LO is introduced aiming at getting the correct binding energy of  ${}^6\text{He}$  and to eliminate cutoff dependencies on the two-body potentials.

The constructed EFT non-local  $\alpha - n$  potential binds a bound state in the  $S$ -wave that simulates a forbidden state. As this state gives spurious eigenvalues in the three-body Hamiltonian, we must remove it. In this paper, we address the elimination of forbidden states in cluster EFT potentials by extending the projection technique given in Ref. [19] to non-local potentials.

The paper is organized as follows. In sec. II, we describe the three-body model with non-local potentials in hyperspherical coordinates. Section III summarizes the derivation of the two-body potentials. In Sec. IV, we describe the calculation of the dipole strength distribution. Section V shows the application to  ${}^6\text{He}$ . Concluding remarks are given in Sec. VI.

## II. THREE-BODY MODEL WITH NON-LOCAL POTENTIALS

### A. Coupled differential equations in hyperspherical coordinates

Let us consider a three-body nucleus, made of three clusters, each with nucleon numbers  $A_i$  and position coordinates  $\mathbf{r}_i$ . The Hamiltonian of the system, for two-cluster interactions only, is given by

$$H = \sum_{i=1}^3 \frac{\mathbf{p}_i^2}{2m_N A_i} + \sum_{i<j=1}^3 V_{ij}, \quad (1)$$

with  $m_N$  the nucleon mass and  $\mathbf{p}_i$  the momentum of cluster  $i$ .

After removing the center of mass motion, we need to solve

$$H_{3b}\Psi^{JM\pi} = E\Psi^{JM\pi}, \quad (2)$$

with  $E$  the three-body energy measured from the three-body breakup threshold. The function  $\Psi^{JM\pi}$  is an eigenstate of the three-body Hamiltonian with total angular momentum  $J$ , projection on the  $z$ -axis  $M$  and parity  $\pi$ . Variational solutions of Eq. (2) with  $E < 0$  are bound states and with  $E > 0$  are the so-called pseudostates.

Aiming at solving Eq. (2), we make use of the scaled Jacobi coordinates [10]

$$\begin{aligned} \mathbf{x}_k &= \sqrt{\mu_{ij}}(\mathbf{r}_j - \mathbf{r}_i), \\ \mathbf{y}_k &= \sqrt{\mu_{(ij)k}} \left( \mathbf{r}_k - \frac{A_i \mathbf{r}_i + A_j \mathbf{r}_j}{A_i + A_j} \right), \end{aligned} \quad (3)$$

with  $(i, j, k)$  a cyclic permutation of  $\{1, 2, 3\}$ . Thus, we have three sets of scaled Jacobi coordinates. The dimensionless reduced masses  $\mu_{ij}$  and  $\mu_{(ij)k}$  are defined as

$$\mu_{ij} = \frac{A_i A_j}{A_i + A_j}, \quad \mu_{(ij)k} = \frac{(A_i + A_j) A_k}{A_i + A_j + A_k}. \quad (4)$$

Each of the three sets of scaled Jacobi coordinates in Eq. (3) defines the hyperspherical coordinates

$$\begin{aligned} \rho^2 &= x_k^2 + y_k^2, \\ \alpha_k &= \arctan\left(\frac{y_k}{x_k}\right); \quad 0 \leq \alpha_k \leq \pi/2, \\ \Omega_{x_k} &= (\theta_{x_k}, \varphi_{x_k}), \quad \Omega_{y_k} = (\theta_{y_k}, \varphi_{y_k}), \end{aligned} \quad (5)$$

where  $\rho$  and  $\alpha_k$  are called the hyperradius and the hyperangle, respectively.

In the hyperspherical formalism, the eigenstate  $\Psi^{JM\pi}$  is expanded in hyperspherical harmonics,  $\mathcal{Y}_{\gamma K}^{JM}(\Omega_{5_k})$ , as

$$\Psi^{JM\pi}(\rho, \Omega_{5_k}) = \rho^{-5/2} \sum_{K=0}^{\infty} \sum_{\gamma} \chi_{\gamma K}^{J\pi}(\rho) \mathcal{Y}_{\gamma K}^{JM}(\Omega_{5_k}), \quad (6)$$

where  $\chi_{\gamma K}^{J\pi}(\rho)$  is the hyperradial wave function and the hyperspherical harmonics  $\mathcal{Y}_{\gamma K}^{JM}(\Omega_{5_k})$  are given by

$$\mathcal{Y}_{\gamma K}^{JM}(\Omega_{5_k}) = \left[ \mathcal{Y}_L^{l_x l_y K}(\Omega_{5_k}) \otimes \chi_S \right]^{JM}, \quad (7)$$

with  $\Omega_{5_k} = (\Omega_{x_k}, \Omega_{y_k}, \alpha)$  and  $\chi_S$  the spin wave function of the three bodies. The term  $\mathcal{Y}_{l_x l_y K}^{LM_L}(\Omega_5)$  is defined as the following coupling

$$\mathcal{Y}_{l_x l_y K}^{LM_L}(\Omega_5) = \phi_K^{l_x l_y}(\alpha) [Y_{l_x}(\Omega_x) \otimes Y_{l_y}(\Omega_y)]^{LM_L}, \quad (8)$$

where we have omitted the subindex  $k$  and where the function  $\phi_K^{l_x l_y}(\alpha)$  is given in Ref. [10].

Index  $\gamma$  in Eq. (6) stands for  $\gamma = (l_x, l_y, L, S)$ , with  $l_x$  and  $l_y$  the orbital angular momenta associated with a set of Jacobi coordinates in Eq. (3),  $L$  is the total orbital angular momentum coupled to  $l_x$  and  $l_y$ , and  $S$  is the total spin of the clusters. The parity of a state is given by  $\pi = (-1)^K$ . In numerical calculations, the hypermomentum  $K$  is truncated at a  $K_{\max}$  value.

After inserting Eq. (6) into the Schrödinger equation for two-cluster non-local potentials only, we end up with the set of coupled differential equations [18]

$$\begin{aligned} \left( -\frac{\hbar^2}{2m_N} \left[ \frac{d^2}{d\rho^2} - \frac{(K+3/2)(K+5/2)}{\rho^2} \right] - E \right) \chi_{\gamma K}^{J\pi}(\rho) \\ + \sum_{K'\gamma'} \int_0^{\infty} W_{\gamma K, \gamma' K'}(\rho, \rho') \chi_{\gamma' K'}^{J\pi}(\rho') d\rho' = 0. \end{aligned} \quad (9)$$

The non-local kernel  $W_{\gamma K, \gamma' K'}(\rho, \rho')$  in Eq. (9) is given by

$$\begin{aligned} W_{\gamma K, \gamma' K'}(\rho, \rho') &= \sum_{k=1}^3 \sum_{l'_x l''_y} (\rho \rho')^{-3/2} \mu_{ij}^{-3/2} \delta_{LL'} \delta_{SS'} \\ &\quad \times \langle k, l'_x l''_y | i, l_x l_y \rangle_{KL} \\ &\quad \times \langle k, l'_x l''_y | i, l'_x l'_y \rangle_{KL} \mathcal{I}(\rho, \rho'), \end{aligned} \quad (10)$$

with the integral  $\mathcal{I}(\rho, \rho')$  defined as

$$\mathcal{I}(\rho, \rho') = \int_0^{\min(\rho, \rho')} W_k^{l''} \left( \frac{x}{\sqrt{\mu_{ij}}}, \frac{x'}{\sqrt{\mu_{ij}}} \right) \phi_K^{l'' l'''}(\alpha) \phi_{K'}^{l'' l'''}(\alpha) x x' y^2 dy. \quad (11)$$

In Eq. (11), the  $W_k^{l''} \left( \frac{x}{\sqrt{\mu_{ij}}}, \frac{x'}{\sqrt{\mu_{ij}}} \right)$  term is a non-local cluster-cluster interaction,  $x = (\rho^2 - y^2)^{1/2}$ ,  $x' = (\rho'^2 - y^2)^{1/2}$ ,  $\alpha = \arctan(y/x)$ ,  $\alpha' = \arctan(y/x')$ . The  $\langle k, l'' l'' | i, l_x l_y \rangle_{KL}$  in Eq. (10) are the Raynal-Revai coefficients [20]. These coefficients allow to transform the hyperspherical harmonics that depend on the set of coordinates  $i$  to the set of coordinates  $k$ .

### B. Diagonalization of the Hamiltonian with the Lagrange mesh technique

The Lagrange mesh technique is a variational calculation on a mesh [21]. This efficient technique simplifies the calculations of the Hamiltonian matrix elements, when they are computed at the Gauss approximation associated with the mesh. Therefore, with this technique the kinetic matrix elements become analytical and the matrix elements for local potentials are diagonal and evaluated at the mesh points.

Let us use the Lagrange-mesh technique to solve Eq. (9) when non-local potentials are involved. That is, we expand the hyperradial wave function  $\chi_{\gamma K}^{J\pi}(\rho)$  over a set of  $N$  regularized Lagrange-Laguerre functions  $\hat{f}_n \left( \frac{\rho}{h} \right)$  as

$$\chi_{\gamma K}^{J\pi}(\rho) = \frac{1}{\sqrt{h}} \sum_{n=1}^N C_{\gamma K n}^{J\pi} \hat{f}_n \left( \frac{\rho}{h} \right), \quad (12)$$

where the  $C_{\gamma K n}^{J\pi}$  are the coefficients of the expansion,  $h$  is a scaling parameter that allows to adjust the mesh to the size of the physical system, and the basis functions  $\hat{f}_n \left( \frac{\rho}{h} \right)$  are given in Ref. [10].

After inserting the expansion (12) into the set of coupled differential equations (9) and projecting onto  $\frac{1}{\sqrt{h}} \hat{f}_n \left( \frac{\rho}{h} \right)$ , we get the eigenvalue problem

$$\sum_{\gamma' K' n'} (T_{\gamma K n, \gamma' K' n'}^{J\pi} + W_{\gamma K n, \gamma' K' n'}) C_{\gamma' K' n'}^{J\pi} - E \delta_{\gamma \gamma'} \delta_{K K'} \delta_{n n'} C_{\gamma' K' n'}^{J\pi} = 0, \quad (13)$$

with  $T_{\gamma K n, \gamma' K' n'}^{J\pi}$  defined as

$$T_{\gamma K n, \gamma' K' n'}^{J\pi} = \frac{\hbar^2}{2m_N} \left( \frac{\hat{T}_{nn'}}{h^2} + \frac{(K + \frac{3}{2})(K + \frac{5}{2})}{u_n^2 h^2} \delta_{nn'} \right) \delta_{\gamma \gamma'} \delta_{K K'}. \quad (14)$$

The kinetic matrix elements  $\hat{T}_{nn'}^G$  of the Lagrange-Laguerre basis are given in Ref. [10]. The potential matrix elements  $W_{\gamma K n, \gamma' K' n'}$  become

$$W_{\gamma K n, \gamma' K' n'} = \frac{1}{h} \int_0^\infty d\rho \int_0^\infty d\rho' \hat{f}_n \left( \frac{\rho}{h} \right) W_{\gamma K, \gamma' K'}(\rho, \rho') \hat{f}_{n'} \left( \frac{\rho'}{h} \right), \quad (15)$$

where the numerical computation is performed following the appendix of Ref. [18].

## III. TWO-BODY EFT POTENTIALS

### A. Derivation

The construction of an EFT starts with the finding of the most general Lagrangian of the system. This Lagrangian must be consistent with all the symmetries in terms of the relevant effective degrees of freedom in the energy regime considered. Galilean-invariant operators in the Lagrangian depend on the relative momenta  $\hbar \mathbf{k}$  and  $\hbar \mathbf{k}'$ , only. Thus, the potential can be written as a series of contact interactions and their derivatives, i.e., at low energies in momentum space, we can write

$$V(\mathbf{k}, \mathbf{k}') = \sum_{l=0}^{\infty} (2l+1) V_l(k, k') P_l(\hat{\mathbf{k}}, \hat{\mathbf{k}}'), \quad (16)$$

where  $P_l$  is a Legendre polynomial of degree  $l$  and where the partial wave term of the potential  $V_l$  is written as

$$V_l(k, k') = k^l k'^l g(k) g(k') \sum_{\alpha\beta=0}^1 k^{2\alpha} \lambda_{\alpha\beta} k'^{2\beta}. \quad (17)$$

The matrix elements  $\lambda_{\alpha\beta}$  are defined in the matrix

$$\lambda = \begin{pmatrix} \lambda_0 & \lambda_1 \\ \lambda_1 & 0 \end{pmatrix}. \quad (18)$$

Note that the limits of the sums over the indexes  $\alpha$  and  $\beta$  in Eq. (17) could be larger than one. However, we are restricting these sums up to  $k^2$  terms as it will be explained later.

The factor

$$g(k) = e^{-(k/\Lambda)^{2m}}, \quad (19)$$

in Eq. (17) is a regularization function, where  $\Lambda$  is called the cutoff parameter. This parameter suppresses high momenta components, that is,  $g(k) \rightarrow 0$  when  $\Lambda \rightarrow \infty$ . However to get  $\lambda_0$  and  $\lambda_1$  finite,  $\Lambda$  must also be finite and limited by the Wigner bound [22]. In principle, observables should not depend on  $\Lambda$ . The coefficients  $\lambda_0$  and  $\lambda_1$  in Eq. (18) are the so-called low energy constants (LECs) that capture the effects from high-energy physics.

The main idea is to find the LECs in Eq. (17) from the matching with a low energy theory. To this end, we make use of the partial wave expansion of the Lippmann-Schwinger equation of the  $T$ -matrix [23]

$$T_l(k, k') = V_l(k, k') + \frac{1}{2\pi^2} \times \int_0^\infty dq q^2 V_l(k, q) \frac{1}{\frac{\hbar^2 k^2}{2\mu} - \frac{\hbar^2 q^2}{2\mu} + i\epsilon} T_l(q, k'), \quad (20)$$

where  $\mu$  is the reduced mass of the two clusters. Here, the  $T$ -matrix is expanded as in Eq. (16) and the free state  $|\mathbf{k}\rangle$  is normalized as

$$\langle \mathbf{k} | \mathbf{k}' \rangle = (2\pi)^3 \delta(\mathbf{k} - \mathbf{k}'). \quad (21)$$

The LECs  $\lambda_0$  and  $\lambda_1$  are found when the potential (17) is introduced in Eq. (20) and it is matched with the on-shell partial wave of the  $T$ -matrix  $T_l$

$$T_l = -\frac{2\pi\hbar^2}{\mu} \left( -\frac{1}{a_l} + \frac{1}{2} r_l k^2 - i k^{2l+1} \right)^{-1} k^{2l}. \quad (22)$$

Equation (22) is derived from the the effective range expansion (ERE) for uncharged cluster-cluster interactions [24, 25]

$$k^{2l+1} \cot \delta_l = -\frac{1}{a_l} + \frac{1}{2} r_l k^2 + \dots \quad (23)$$

In Eq. (23)  $\delta_l$  is the phase-shift for the elastic scattering in the partial wave  $l$ . The  $a_l$  and  $r_l$  are the so-called scattering length and effective range parameters, in units of  $\text{fm}^{2l+1}$  and  $\text{fm}^{-2l+1}$ , respectively. We consider terms up to the effective range i.e., up to  $k^2$ , which limits the indexes of the sums in Eq. (17) up to 1. Once the experimental values of  $a_l$  and  $r_l$  are introduced in Eq. (22) in combination with an appropriate power counting, the LECs  $\lambda_0$  and  $\lambda_1$  are obtained (see the Appendix for a summary and Refs. [15–17] for details).

Equation (11) involves partial waves of cluster-cluster potentials in coordinate representation. They can be obtained from the EFT potentials of the form (16) by the double Fourier transform

$$V(\mathbf{r}, \mathbf{r}') = \frac{1}{(2\pi)^3} \int d\mathbf{k} d\mathbf{k}' e^{-i(\mathbf{r}\cdot\mathbf{k} + \mathbf{r}'\cdot\mathbf{k}')} V(\mathbf{k}, \mathbf{k}'). \quad (24)$$

Expanding  $V(\mathbf{r}, \mathbf{r}')$  and  $V(\mathbf{k}, \mathbf{k}')$  in partial waves as shown in Eq. (16), and with the help of the plane wave expansion in spherical waves, we have that each partial wave satisfies

$$V_l(r, r') = (-1)^l \frac{2}{\pi} \int_0^\infty \int_0^\infty dk dk' k^2 k'^2 j_l(kr) V_l(k, k') j_{l'}(k'r'). \quad (25)$$

In Eq. (25)  $j_l(kr)$  is a spherical Bessel function of the first kind.

## B. Forbidden states

The concept of forbidden states shows up in many-body theories of fermions, since the full antisymmetrization of the wave function must be taken into account. For two-cluster nuclei, the Pauli principle can be considered approximately by choosing deep nucleus-nucleus interactions containing unphysical bound states that simulate the forbidden states [26]. These forbidden states are located at energies  $E_F$  lower than the physical ones.

When we are treating three-body nuclei, the two-body forbidden states add spurious eigenvalues associated with the three-body Hamiltonian that need to be removed. Different techniques such as the supersymmetry transform of the nucleus-nucleus potential [27] or the projection technique [19] have been introduced to remove forbidden states in local nucleus-nucleus potentials. These transformations keep the phase shifts unaffected.

In this paper, we extend the projection technique [19] to non local potentials by substituting  $V_l(k, k')$  in Eq. (17), for the  $l = 0$   $\alpha - n$  potential, by

$$V_l(k, k') = V_l(k, k') + \Gamma \phi_l(k) \phi_l(k'), \quad (26)$$

where  $\Gamma$  is a large constant energy value (typically  $\Gamma \sim 10^3 - 10^9$  MeV). The function  $\phi_l(k)$  is a forbidden state or an eigenstate of the nucleus-nucleus Hamiltonian with eigenvalue  $E_F$ . Thus,  $\phi_l(k)$  is orthogonal to the physical bound states.

## IV. E1 STRENGTH DISTRIBUTION

Electric dipole excitations of weakly bound nuclei with just one bound state go directly to the continuum. If such nuclei are made of two-clusters, the calculation of the E1 strength distribution is rather simple [28]. However, for three-body nuclei, the computation of the three-body continuum with the correct asymptotic behavior, which is needed to compute E1 strength distributions, may involve rather heavy calculations such as solving the Faddeev equations in the continuum [29] or the  $R$ -matrix method [30]. There are other methods that extend the application of bound state variational calculations to the continuum. They are the complex scaling [31, 32], particularly suitable to treat resonant continuum regions, and integral transform (LIT) methods also in non-resonant energy regions [33, 34]. Another widely used technique is the so-called pseudostate approach [32, 35–37].

In Refs. [32, 36] the E1 strength distribution of  ${}^6\text{He}$  is computed in a three-body model with hyperspherical coordinates and two-body local potentials. The complex scaling and the pseudostate methods are tested with a computation that includes the correct asymptotic behavior of the continuum. These references show very good agreement among the computation with the exact continuum and the discretized approaches, although some ambiguity exists in the pseudostate method due to the

smoothing technique necessary to derive continuous distributions. In the following we briefly explain the pseudostate method and clarify that no ambiguity exists when it is used within an integral transform approach.

We start following the definition of the three-body dipole strength distribution [11]

$$\frac{dB_{E1}}{dE}(E) = \frac{1}{2J_0 + 1} \delta(E - \mathcal{E}) \sum_{JM\pi M_0\mu} \sum_{\gamma\omega K\omega} \left| \langle \mathcal{K} \Psi_{\gamma\omega K\omega}^{JM\pi}(\mathcal{E}) | \mathcal{M}_{\mu}^{(E1)} | \Psi^{J_0 M_0 \pi_0} \rangle \right|^2, \quad (27)$$

where  $\Psi^{J_0 M_0 \pi_0}$  is the initial bound state characterized by total angular momentum, projection on the  $z$  axis and parity,  $J_0$ ,  $M_0$ , and  $\pi_0$ , respectively. The final unbound state is represented by  $\Psi_{\gamma\omega K\omega}^{JM\pi}(\mathcal{E})$ , with total angular momentum  $J$ , angular momentum projection  $M$  and parity  $\pi$ , where  $\mathcal{K}$  is the time-reversal operator and  $E$  is the excitation energy defined from the three-body breakup threshold. Note that here we have defined the response function with a Dirac Delta function to be further introduced into an integral transform.

The electric dipole operator for a core +  $n$  +  $n$  system, with the Jacobi coordinate  $\mathbf{x}$  along the  $n$  -  $n$  motion (see Ref. [10] for details), is given by

$$\mathcal{M}_{\mu}^{E1}(\alpha, \rho) = eZ_c \left( \frac{2}{AA_c} \right)^{1/2} \rho \sin \alpha Y_1^{\mu}(\Omega_y), \quad (28)$$

with  $A_c$  and  $eZ_c$  the nucleon number and charge of the core, and  $A = A_c + 2$ .

On the other hand, an observable in an experiment is measured with a resolution defined by the experimental apparatus [38]. The latter can be represented in various forms. We will use a generical function  $K_{resol}(E, \mathcal{E}, \Gamma \dots)$ , where  $\mathcal{E}, \Gamma \dots$  are the parameters of the resolution function. For example, if it is represented by a Gaussian or a Lorentzian function,  $\mathcal{E}$  and  $\Gamma$  could be the center and the width of those functions. In principle  $\Gamma$  could also depend on  $E$ . We take it constant for simplicity of the presentation.

Therefore, because of the experimental resolution, one actually measures the following integral transform of the dipole strength

$$\frac{dB_{E1}}{dE}(\mathcal{E}) = \int dE \frac{dB_{E1}}{dE}(E) K_{resol}(E, \mathcal{E}, \Gamma \dots). \quad (29)$$

Then, introducing the theoretical E1 strength distribution (27) in Eq. (29) and inserting the completeness relation of states that diagonalizes the three-body Hamiltonian, one can show that for the case of the Borromean nucleus  ${}^6\text{He}$ , that has  $J_0^{\pi} = 0^+$  and  $J^{\pi} = 1^-$ , we obtain [39, 40]

$$\frac{dB_{E1}}{dE} = \sum_{\lambda} | \langle \Psi_{\lambda}^{1M^-}(\mathcal{E}_{\lambda}) | \mathcal{M}^{E1} | \Psi^{00+} \rangle |^2 K_{resol}(E, \mathcal{E}_{\lambda}, \Gamma \dots). \quad (30)$$

The  $\Psi_{\lambda}^{1M^-}(\mathcal{E}_{\lambda})$  are pseudostates or eigenstates of the three-body Hamiltonian at positive energies  $\mathcal{E}_{\lambda}$ , for the partial wave  $J^{\pi} = 1^-$ .

What is important here is that for general positive definite Kernels such as Lorentzians or Gaussians, and the easily verified conditions about the existence of the transform and of the total strength, a theorem ensures that the transform can be calculated by means of finite norm functions (the pseudostates) [39, 40]. The smoothed discretized distribution, namely the integral transform, converges exactly to the experimental folded strength distribution, at sufficiently high number of pseudostates. It has been noticed that the experimental smoothing procedure excludes higher-frequency oscillations, which therefore are irrelevant. On the other hand, theoretical results that show isolated Lorentzian/Gaussian peaks may indicate that the corresponding structure is not sufficiently resolved. Therefore an enlargement of the basis space is necessary.

Response functions can be obtained from the inversion of integral transforms [41]. However, we would like to emphasize that if a smooth theoretical result is obtained with the experimental resolution, an inversion of the transform is not necessary. Problems can only arise if the experimental resolution is so small that such a smooth result is not obtained and isolated peaks due to single pseudostates appear, even if the basis is enlarged. In such a case it is more reliable to use an inversion for the transform [42].

## V. ${}^6\text{He}$ STRUCTURE

### A. Two-body potentials

The derivation of the LECs  $\lambda_0$  and  $\lambda_1$  for the two-cluster potential (17) is performed in Refs. [15–17] and is summarized in the Appendix. We use the experimental values of the scattering length  $a_l$  and the effective range  $r_l$  cited in Table I. They are taken from Refs. [43, 44] for the  $n$  -  $n$  system, and from Ref. [45] for the  $\alpha$  -  $n$  system.

TABLE I. Experimental scattering length and effective range parameters to obtain two-body EFT potentials.

System	$l_j$	$a_l$ (fm $^{2l+1}$ )	$r_l$ (fm $^{-2l+1}$ )
$n + n$	$S_0$	$-18.630 \pm 0.480$	$2.870 \pm 0.100$
$\alpha + n$	$S_{1/2}$	$2.464 \pm 0.004$	$1.385 \pm 0.041$
$\alpha + n$	$P_{3/2}$	$-62.951 \pm 0.003$	$-0.882 \pm 0.001$

Once the EFT potentials are calculated in momentum space, they are transformed to coordinate representation by performing a double Fourier transform as indicated in Eq. (25). The integrals are computed numerically with the help of a double Gauss-Legendre quadrature of  $N_k = 300$  points.

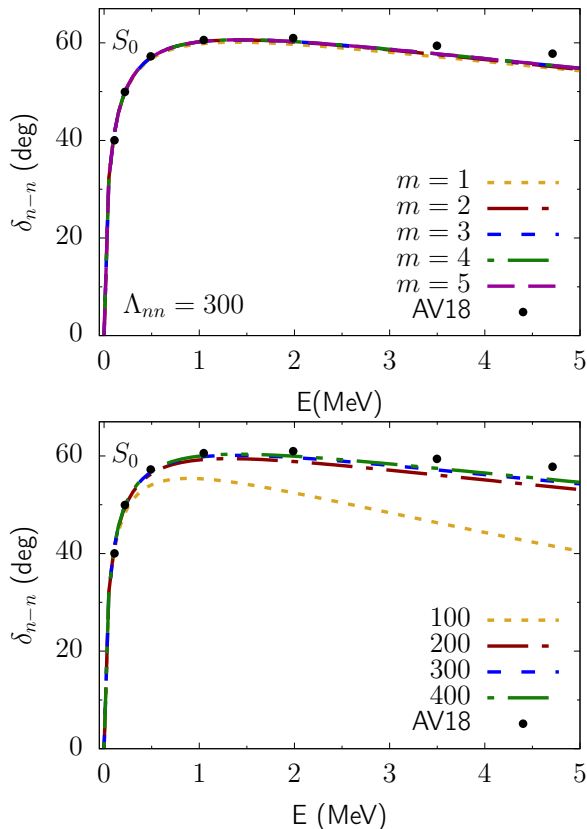


FIG. 1. Dependence of the EFT  $n - n$  phase shift on the exponent of the regularization function (top) and on the cutoff parameter  $\Lambda_{nn}$ , in MeV, in natural units (bottom). The points are the calculations with the AV18 potential [46].

Figure 1 shows the low energy behavior of the  $n - n$   $^1S_0$  phase shift computed with the two-body EFT potentials in comparison with a calculation that uses the AV18 potential [46]. We show the dependence on the exponent  $m$  of the Gaussian regularization function (19) and on the cutoff parameter  $\Lambda_{nn}$ . As mentioned before, this parameter should be as large as possible, limited by the Wigner bound and the physics, in principle, should not depend on it. We observe a slight dependence on the cutoff parameter apart from  $\Lambda_{nn} = 100$  MeV. The low energy phase-shifts for the  $S$ -wave and  $P_{3/2}$   $\alpha - n$  systems are studied in Refs. [15, 16].

In coordinate representation, we calculate the phase shifts with the  $R$ -matrix method for non-local potentials [21]. We also check that the Fourier transformed EFT potentials reproduce the experimental scattering lengths  $a_l$  and the effective range  $r_l$  values. To this end, we extended Ref. [47] to compute effective range parameters with the  $R$ -matrix method for non-local potentials.

Table II gives the set of EFT potential parameters that are used to compute ground state properties of  $^6\text{He}$ , unless mentioned otherwise. We choose  $\Lambda$  values as large as possible avoiding being close to Wigner bounds.

On the other hand, the  $S$ -wave  $\alpha - n$  EFT potential

TABLE II. EFT two-body potential parameters in natural units <sup>a</sup>.

System	$l_j$	$m$	$\Lambda$	$\lambda_0$ (fm $^{2(l+1)}$ )	$\lambda_1$ (fm $^{4+2l}$ )
$n + n$	$S_0$	1	300	-5.320	1.660
$\alpha + n$	$S_{1/2}$	2	400	-6.764	1.311
$\alpha + n$	$P_{3/2}$	1	300	-10.177	2.714

<sup>a</sup> In. S.I units  $\lambda_0 \rightarrow \lambda_0 \hbar c$ ,  $\lambda_1 \rightarrow \lambda_1 \hbar c$  and  $\Lambda \rightarrow \Lambda / \hbar c$ , where  $\hbar c = 197.3$  MeVfm.

binds a forbidden state. We remove this state by adding a projector to the potential in momentum space as indicated in Eq. (26). The functions  $\phi(k)$  are obtained by solving the Schrödinger equation in momentum space following Ref. [48] with  $N_p = 30$  Lagrange-Laguerre basis functions and scaling parameter  $h_p = 0.3$  fm. We have checked that the phase shifts remain unaffected with the addition of the projector potential. Once we have the potential (26), we proceed to perform its double Fourier transform. Table III shows the  $S$ -wave  $\alpha - n$  potential parameters for  $m = 2$  and different cutoff parameters  $\Lambda_{\alpha n}^0$ . We also show the associated forbidden state energies. These energies agree with the value of 12.38 MeV given by the Kanada et al. local potential [49] used in Ref. [10].

TABLE III. EFT potential parameters, in natural units, and forbidden state energies for  $S$ -wave  $\alpha - n$  potentials with  $m = 2$ .

$\Lambda_{\alpha n}^0$ (MeV)	$\lambda_0$ (fm $^{2(l+1)}$ )	$\lambda_1$ (fm $^{2l+4}$ )	$E_F$ (MeV)
200	-2.031	-7.331	-5.68
300	-6.963	0.807	-12.34
400	-6.764	1.311	-13.45
500	-6.290	2.005	-13.99

## B. $\alpha + n + n$ ground state properties

The two-body potentials with parameters given in Table II are used in Eq. (13) to compute the ground state energy,  $E_0$ , of  $^6\text{He}$ . We solve the diagonalization problem as shown in Ref. [18] with  $N = 60$  mesh points and scaling parameter  $h = 0.3$  fm. The integrals over  $x$  and  $x'$  are computed with a Gauss-Laguerre quadrature with  $N_2 = 30$  and  $h_2 = 0.3$  fm. The integral over  $y$  is performed with  $N_y = 250$  points and a step of  $h_y = 0.05$  fm.

The two-body potentials alone do not bind the system. Therefore, we introduce the three-body force

$$V_3(\rho) = -V_{03} e^{-\left(\frac{\rho}{\rho_0}\right)^2}, \quad (31)$$

which corresponds to a  $S$ -wave LO cluster EFT potential in coordinate representation. In Eq. (31)  $\rho_0$  makes the

role of a three-body cutoff parameter. The introduction of this force allows to reproduce the correct experimental ground state energy and to remove dependencies on this energy of the cutoff parameter of the two-body EFT potentials.

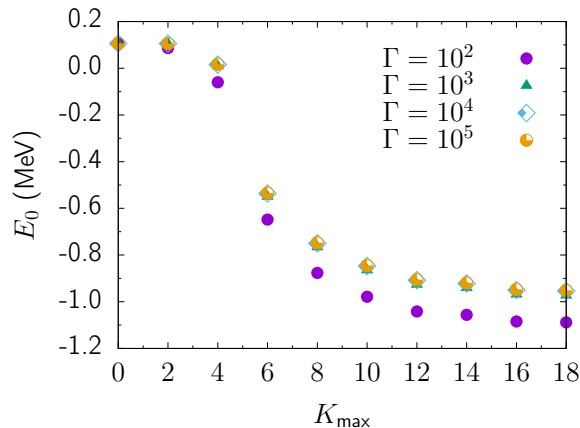


FIG. 2. Convergence with  $K_{\max}$  of the ground state energy of  ${}^6\text{He}$  for different values of the projector parameter  $\Gamma$  in MeV.

In Fig. 2, we study the convergence of  $E_0$  with respect to the maximum  $K$  value,  $K_{\max}$ , in the expansion (6) of the three-body wave function. We also check the dependence of this energy on the projector  $\Gamma$  at eliminating the forbidden state in the  $S_{1/2}$  non-local  $\alpha - n$  potential. As it is the case for local potentials [10],  $\Gamma$  values at least of 1000 MeV are needed to eliminate dependencies of the ground state energy. We use  $V_{03} = -15.2$  MeV and  $\rho_0 = 5$  fm to obtain the theoretical value of  $-0.979$  MeV, which is close to the experimental value  $-0.97546(23)$  MeV [50].

We also compute the rms radius of the  $\alpha + n + n$  system through the expression [8]

$$\langle r^2 \rangle_{6\text{He}} = \frac{1}{6} \langle \Psi^{J_0 M_0 \pi_0} | \rho^2 | \Psi^{J_0 M_0 \pi_0} \rangle + \frac{2}{3} \langle r^2 \rangle_{\alpha}, \quad (32)$$

with  $\Psi^{J_0 M_0 \pi_0}$  the ground state of  ${}^6\text{He}$  and  $\sqrt{\langle r^2 \rangle_{\alpha}}$  the rms radius of the  ${}^4\text{He}$  nucleus. For this radius we take the experimental value of 1.463(6) fm given in Ref. [51]. With the three-body ground state mentioned before, we reproduce the value of 2.81 fm for the rms radius of  ${}^6\text{He}$ . This value is in fair agreement with the experimental measurement of 2.49(4) fm [52].

### C. Electric dipole strength distribution

In this section we compute the electric dipole strength distribution of  ${}^6\text{He}$  using Eq. (30). We employ a Gaussian smoothing distribution with  $\sigma = (0.027 + 0.177E^{0.654})$  MeV, which corresponds to the experimental energy resolution [52]. This distribution is normalized to unity from 0 to  $\infty$ . We use the same Hamiltonian and numerical

conditions to compute the ground and the  $1^-$  discrete states.

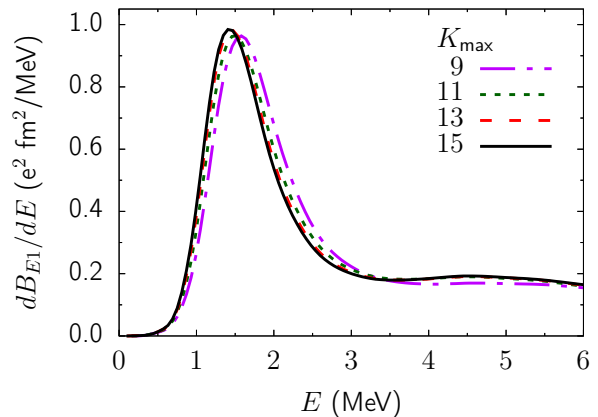


FIG. 3. Convergence of the E1 strength distribution of  ${}^6\text{He}$  with  $K_{\max}$ .

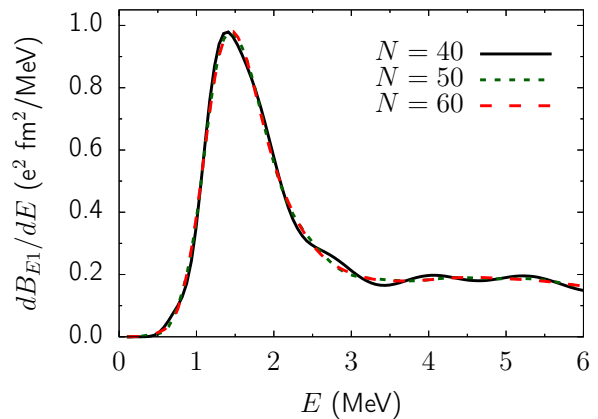


FIG. 4. Convergence of the E1 strength distribution of  ${}^6\text{He}$  with the number of the Lagrange-Laguerre basis functions  $N$ .

Figure 3 shows the convergence of the E1 strength distribution with the maximum value of the hypermomentum  $K_{\max}$  of the  $1^-$  pseudostates. We observe that we achieve convergence at  $K_{\max} = 13$ . In Fig. 4 we show the convergence of the E1 strength distribution with the number of the Lagrange-Laguerre basis functions involved in the diagonalization of the three-body Hamiltonian with non-local potentials. The number of pseudostates corresponds to 242, 395 and 525 for  $N = 40$ ,  $N = 50$  and  $N = 60$ , respectively. As isolated resonances are not obtained at increasing the number of pseudostates in the sum (30), we do not need to perform an inversion of the integral transform (29).

Aiming at assessing the effect of the cutoff parameter of the two-cluster potentials on the E1 strength distribution, we compute this quantity for different values of the  $\Lambda_{nn}$ ,  $\Lambda_{\alpha n}^0$  and  $\Lambda_{\alpha n}^1$  cutoff parameters of the  $S_0$   $n-n$ ,  $S_{1/2}$   $\alpha-n$  and  $P_{3/2}$   $\alpha-n$  potentials, respectively. We observe

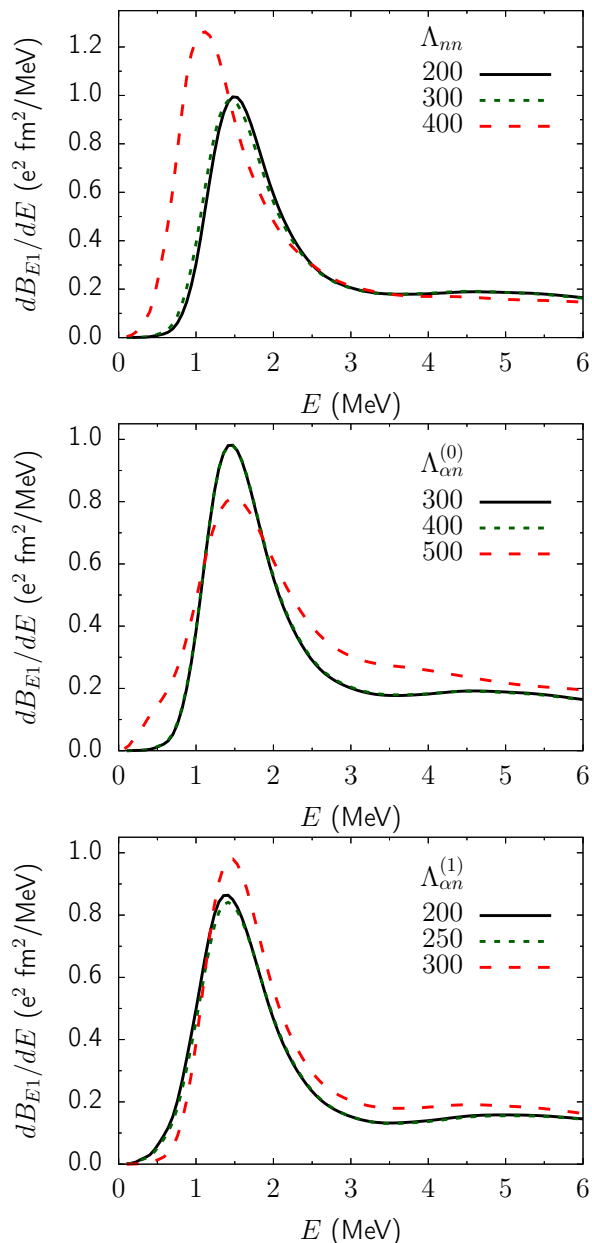


FIG. 5. Influence of the cutoff parameter, labels in MeV, in natural units, of the two-body potentials, on the E1 strength distribution of  ${}^6\text{He}$ .

a strong dependence on the E1 transition distribution for the values  $\Lambda_{nn} = 400$  MeV,  $\Lambda_{\alpha n}^0 = 500$  MeV and  $\Lambda_{\alpha n}^1 = 300$  MeV, which are close to the Wigner bounds 410 MeV, 510 MeV and 340 MeV of the  $S_0$   $n-n$ ,  $S_{1/2}$   $\alpha-n$  and  $P_{3/2}$   $\alpha-n$  potentials, respectively. We also find that the ground state of  ${}^6\text{He}$  exhibits a slow convergence with  $K_{\max}$  ( $K_{\max} = 30$ ), when the two-body potentials have a cutoff parameter that tends to a Wigner bound. In addition, we check the dependence of the E1 strength with the exponent  $m$  of the regularization function (19). We get that this quantity differs at most 10% for all po-

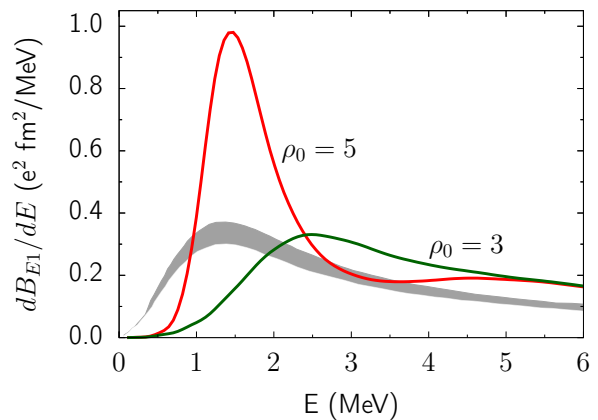


FIG. 6. Sensitivity of the E1 strength distribution of  ${}^6\text{He}$  with  $\rho_0$  (in fm). Experimental data given by the shade area [52].

tentials in the peak region. In general, the EFT  ${}^6\text{He}$  E1 strength distributions are in good agreement with the computation of the three-body model with phenomenological two-body local potentials of Ref. [11].

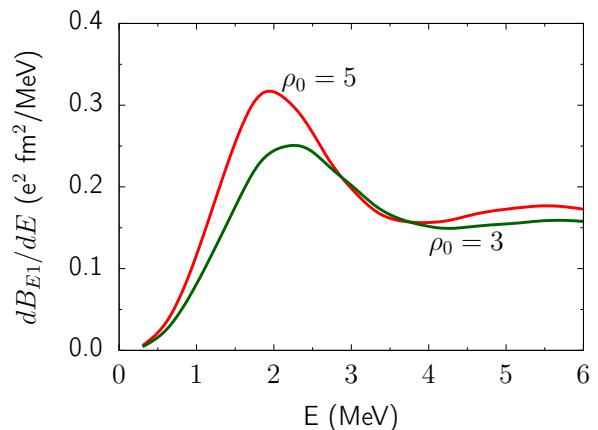


FIG. 7. Sensitivity of the E1 strength distribution of  ${}^6\text{He}$  with  $\rho_0$  (in fm), when two-body local phenomenological potentials are used.

In Fig. 6, we show the dependence of the electric dipole strength distribution with  $\rho_0$ , i.e., with the cutoff parameter of the  $S$ -wave LO three-body potential. We use the values  $\rho_0 = 3$  fm and  $\rho_0 = 5$  fm. With  $\rho_0 = 3$  fm, we need a depth of -47.5 MeV to reproduce the ground state energy of  ${}^6\text{He}$ . This three-body potential provides a rms radius of 2.54 fm. We observe a strong dependence on the three-body cutoff parameter. This dependence could be related with the choice of the three-body interaction. We use a LO  $S$ -wave interaction, since its introduction in hyperspherical coordinates in configuration space is straightforward, and has the same functional form commonly used in three-body calculations with phenomenological local potentials [53, 54]. However, as the  ${}^6\text{He}$  structure is dominated by the  $\alpha-n$   $P_{3/2}$  resonance



the use of a  $P$ -wave three-body potential in our EFT three-body model may be more suitable. Refs. [13, 55] introduce a three-body  $P$ -wave interaction in momentum space. However, its introduction in the coordinate representation is not direct and out of the scope of the present paper.

Although the shape of the  $S$ -wave LO three-body interaction (31) is the same as the one used for three-body calculations with two-body local phenomenological potentials, its effect is different. Fig. 7 shows the dependence on  $\rho_0$  of the E1 strength distribution of  ${}^6\text{He}$ , computed with the three-body model of Refs. [32, 36]. We employ the same potentials and numerical conditions. However, for the sake of simplicity in the comparison, we just use  $K_{\text{max}} = 9$  for the final state. Higher values will shift the peak position to lower energies. To reproduce the experimental ground state energy of  ${}^6\text{He}$ , we tuned the depth of the potential to  $-7$  MeV and  $-2.5$  MeV, which corresponds to  $\rho_0 = 3$  fm and for  $\rho_0 = 5$  fm, respectively. With these three-body potentials, we find the rms radius of 2.39 fm and 2.47 fm. From Fig. 7 we observe that the dependence of the E1 strength on  $\rho_0$  is not as strong as for the case of EFT derived potentials.

## VI. SUMMARY AND CONCLUSIONS

We have studied three-body systems with cluster EFT two-body potentials in coordinate representation, instead of momentum space, where the potentials are naturally derived. Besides avoiding complications with the Coulomb interaction, this will allow to introduce the three-body wave functions into existing low-energy reaction codes. This is necessary to achieve a more fundamental description of reaction processes and to study non-local effects in reaction theory.

To this end, we have started with the  ${}^6\text{He}$  nucleus by using a  $S_0$   $n-n$ , and a  $S_{1/2}$   $\alpha-n$  and  $P_{3/2}$   $\alpha-n$  EFT potentials. We have used a three-body model in hyperspherical coordinates with the Lagrange-mesh technique. The model incorporates the two-body non-local interactions that result from the Fourier transformed cluster EFT potentials in momentum space. We have also addressed the removal of forbidden states in cluster EFT potentials by extending the projection technique [19] to the non-local  $S_{1/2}$   $\alpha-n$  potential. A LO  $S$ -wave three-body interaction is introduced in the Hamiltonian to properly bind the  ${}^6\text{He}$  nucleus and to eliminate dependencies on the two-body cutoff parameter.

Besides the ground state energy of  ${}^6\text{He}$ , we have computed its rms radius and the electric dipole strength distribution. For the latter, we have used the pseudostate approach, which corresponds, under certain conditions, to the integral transform method. In fact, we have compared the results to the experimental data employing the same resolution as in experiment. Such a controlled pseudostate approach, which uses the discretization of the continuum, does not represent an approximation, under

the conditions of the present calculation, and the obtained results can be compared directly to the data. The condition, that an increase in the number of pseudostates exhibits a convergent smooth result without isolated resonances, is verified by our calculation. Therefore an inversion of the transform has not even been necessary.

An EFT should not, in principle, depend on the cutoff parameter of the renormalization function. Thus, we have checked this dependence for the two-body potentials as well as for the three-body interaction. We have observed that the E1 strength distribution depends strongly on the two-body cutoff parameter when it is close to the Wigner bound, requiring a certain care at choosing this value. Moreover we have found a rather strong dependence on the three-body cutoff. It is worth noticing that although its functional form is the same as the one used in the case of three-body calculations with phenomenological potentials, its effect results to be rather different.

Because of the strong dependence on the three-body cut-off the comparison with existing experimental data is problematic. Different from a smaller cutoff a larger cutoff reproduces the energy of the resonance but gives too high a strength. This calls probably for a modification of the three-body interaction (higher order terms or  $P$ -wave interaction). On the other hand the experimental situation is also not yet fully settled. The variation of different experimental results is relatively large. In addition the experimental determination of the dipole strength is strongly model dependent as was pointed out in Ref. [56].

All this makes  ${}^6\text{He}$  still a very interesting and challenging ground for continuing both theoretical and experimental investigations.

## ACKNOWLEDGMENTS

We thank C. Ji, E. Filandri and D. Baron for helping discussions on the EFTs potentials. E. C. Pinilla gratefully acknowledges the support given by the INFN.

### Appendix: LECs under Wigner bound for neutral two-body interactions

In this section, we summarize the derivation of the LECs  $\lambda_0$  and  $\lambda_1$  of the EFT potential (17) in natural units. We refer the reader to Ref. [15–17] for details.

Let us make use of the partial wave expansion of the two-body Lippmann Schwinger equation (20), the partial wave potential (17) and a similar expansion for the  $T$ -matrix

$$T_l(k, k') = k^l k'^l g(k) g(k') \sum_{ij=0}^1 k^{2i} \tau_{ij}(E) k'^{2j}. \quad (\text{A.1})$$

After introducing Eq. (A.1) and Eq. (17) in the Lipp-

mann Schwinger equation (20), we have

$$\begin{aligned} \tau_{ij} &= \lambda_{ij} \\ &+ \frac{1}{2\pi^2} \sum_{i'j'=0}^1 \lambda_{ii'} \int_0^\infty dk k^2 \frac{k^{2l+2i'+2j'}}{E - k^2/2\mu + i\epsilon} g^2(k) \tau_{j'j}, \end{aligned} \quad (\text{A.2})$$

where  $g(k)$  is given by Eq. (19).

Equation (A.2) corresponds to the matrix equation

$$\tau = \lambda + \lambda \Phi^{(l)} \tau, \quad (\text{A.3})$$

with the matrix  $\lambda$  given by Eq. (18) and the matrix  $\Phi^{(l)}$  defined as

$$\Phi^{(l)} = \begin{pmatrix} \phi_0^{(l)} & \phi_2^{(l)} \\ \phi_2^{(l)} & \phi_4^{(l)} \end{pmatrix}. \quad (\text{A.4})$$

The matrix elements of  $\Phi^{(l)}$  are given by the expression

$$\Phi_{2\nu}^{(l)} = \frac{1}{2\pi^2} \int_0^\infty dk k^2 \frac{k^{2l+2\nu}}{E - k^2/2\mu + i\epsilon} g^2(k), \quad (\text{A.5})$$

with  $\nu = 0, 1, 2$ . These matrix elements can be written recursively as

$$\phi_4^{(l)} = I_{2l+5} + k^2 I_{2l+3} + k^4 \phi_0^{(l)}, \quad (\text{A.6})$$

$$\phi_2^{(l)} = I_{2l+3} + k^2 \phi_0^{(l)}, \quad (\text{A.7})$$

$$\phi_{2\nu}^{(l)} = I_{2l+1} + \dots + k^{2l+2} \phi_{-1}^{(l)}, \quad (\text{A.8})$$

where the integral  $I_n$  is given by

$$I_n = -\frac{\mu}{\pi^2} \int_0^\infty dq q^{n-1} g^2(q). \quad (\text{A.9})$$

When the regulator function is defines as in Eq. (19), we have

$$I_n = -\frac{\mu}{\pi^2} \frac{\Lambda^n}{n} f_{n,m}, \quad (\text{A.10})$$

with

$$f_{n,m} = \left(\frac{1}{2}\right)^{\frac{n}{2m}} \Gamma\left(\frac{n}{2m} + 1\right). \quad (\text{A.11})$$

After solving Eq. (A.3), rescaling the the LECs to

$$\lambda_0 = -\frac{\pi^2}{\mu} \frac{c_0}{\Lambda^{2l+1}} \quad \lambda_1 = -\frac{\pi^2}{\mu} \frac{c_1}{\Lambda^{2l+3}}, \quad (\text{A.12})$$

expanding in powers of  $(k/\Lambda)^2$  and comparing with the effective range expression for the on shell  $T$ -matrix (22), we have expressions for the coefficients  $C_0$  and  $C_1$  given by

$$\begin{aligned} c_0 &= \left[ \frac{\left(\frac{f_{3,m}}{3} - \frac{1}{c_1}\right)^2}{f_{1,m} - \frac{\pi}{2a_0\Lambda}} - \frac{f_{5,m}}{5} \right] c_1^2, \\ c_1 &= \left\{ 1 \pm \left[ 1 - \frac{\left(f_{-1,m} - \frac{r_0\pi\Lambda}{4}\right) \frac{f_{3,m}}{3}}{\left(f_{1,m} - \frac{\pi}{2a_0\Lambda}\right)^2} \right]^{-1/2} \right\} \frac{3}{f_{3,m}}, \end{aligned} \quad (\text{A.13})$$

for the  $l = 0$  potentials and

$$\begin{aligned} c_0 &= \left[ \frac{\left(\frac{f_{3,m}}{3} - \frac{1}{c_1}\right)^2}{\frac{f_{3,m}}{3} - \frac{\pi}{2a_1\Lambda^3}} - \frac{f_{7,m}}{7} \right] c_1^2, \\ c_1 &= \left\{ 1 \pm \left[ 1 - \frac{\left(f_{1,m} + \frac{r_1\pi}{4\Lambda}\right) \frac{f_{5,m}}{5}}{\left(\frac{f_{3,m}}{3} - \frac{\pi}{2a_1\Lambda^3}\right)^2} \right]^{-1/2} \right\} \frac{5}{f_{5,m}}, \end{aligned} \quad (\text{A.14})$$

for the  $l = 1$  potentials. The  $a_l$  and  $r_l$  are the experimental scattering length and the effective range associated to the partial wave  $l = 0, 1$ . For each  $l$ , the  $c_1$  constant has two values. The negative root is chosen since it provides the smaller values of most natural size.

- 
- [1] S. Weinberg, *Physica A* **96**, 327 (1979).  
[2] S. Weinberg, *Rev. Mod. Phys.* **52**, 515 (1980).  
[3] P. F. Bedaque and U. van Kolck, *Annu. Rev. Nucl. Part. Sci.* **52**, 339 (2002).  
[4] H.-W. Hammer, C. Ji, and D. R. Phillips, *Journal of Physics G: Nuclear and Particle Physics* **44**, 103002 (2017).  
[5] H.-W. Hammer, S. König, and U. van Kolck, *Rev. Mod. Phys.* **92**, 025004 (2020).  
[6] P. Maris, E. Epelbaum, R. J. Furnstahl, J. Golak, K. Hebeler, T. Hüther, H. Kamada, H. Krebs, U.-G. Meißner, J. A. Melendez, A. Nogga, P. Reinert, R. Roth, R. Skibiński, V. Soloviov, K. Topolnicki, J. P. Vary, Y. Volkotrub, H. Witała, and T. Wolfgruber (LENPIC Collaboration), *Phys. Rev. C* **103**, 054001 (2021).  
[7] J. Al-Khalili, An introduction to halo nuclei, in *The Euroschool Lectures on Physics with Exotic Beams, Vol. I*, edited by J. Al-Khalili and E. Roeckl (Springer Berlin Heidelberg, Berlin, Heidelberg, 2004) pp. 77–112.  
[8] M. V. Zhukov, B. V. Danilin, D. V. Fedorov, J. M. Bang, J. Thompson, and J. S. Vaagen, *Phys. Rep.* **231**, 151 (1993).  
[9] B. V. Danilin, I. J. Thompson, J. S. Vaagen, and M. V. Zhukov, *Nucl. Phys. A* **632**, 383 (1998).  
[10] P. Descouvemont, C. Daniel, and D. Baye, *Phys. Rev. C* **67**, 044309 (2003).  
[11] D. Baye, P. Capel, P. Descouvemont, and Y. Suzuki, *Phys. Rev. C* **79**, 024607 (2009).  
[12] M. Rodríguez-Gallardo, J. M. Arias, J. Gómez-Camacho,

- R. C. Johnson, A. M. Moro, I. J. Thompson, and J. A. Tostevin, Phys. Rev. C **77**, 064609 (2008).
- [13] C. Ji, C. Elster, and D. R. Phillips, Phys. Rev. C **90**, 044004 (2014).
- [14] L. Faddeev, Zh. Eksp. Teor. Fiz **39**, 1014 (1961).
- [15] E. Filandri, P. Andreatta, C. A. Manzata, C. Ji, W. Leidemann, and G. Orlandini, SciPost Phys. Proc. , 034 (2020).
- [16] E. Filandri, *Effective field theory description of  $\alpha$ -cluster nuclei: The  $^9\text{Be}$  ground state and  $^9\text{Be}$  photodisintegration*, Ph.D. thesis, University of Trento (2022).
- [17] Y. Capitani, E. Filandri, C. Ji, and W. Leidemann, in preparation.
- [18] M. Theeten, D. Baye, and P. Descouvemont, Nucl. Phys. A **753**, 233 (2005).
- [19] V. I. Kukulin and V. N. Pomerantsev, Ann. Phys. **111**, 330 (1978).
- [20] J. Raynal and J. Revai, Nuovo Cim. A **39**, 612 (1970).
- [21] D. Baye, Phys. Rep. **565**, 1 (2015).
- [22] E. P. Wigner, Phys. Rev. **98**, 145 (1955).
- [23] C. Joachain, *Quantum Collision Theory* (North-Holland Publishing Company, 1975).
- [24] H. A. Bethe, Phys. Rev. **76**, 38 (1949).
- [25] J. M. Blatt and J. D. Jackson, Phys. Rev. **76**, 18 (1949).
- [26] B. Buck, H. Friedrich, and C. Wheatley, Nucl. Phys. A **275**, 246 (1977).
- [27] D. Baye, Phys. Rev. Lett. **58**, 2738 (1987).
- [28] Y. Suzuki, R. G. Lovas, K. Yabana, and K. Varga, *Structure and Reactions of Light Exotic Nuclei* (Taylor & Francis, London, 2003).
- [29] J. Golak, R. Skibiński, H. Witała, W. Glöckle, A. Nogga, and H. Kamada, Phys. Rep. **415**, 89 (2005).
- [30] P. Descouvemont, E. M. Tursunov, and D. Baye, Nucl. Phys. A **765**, 370 (2006).
- [31] S. Aoyama, T. Myo, K. Katō, and K. Ikeda, Prog. Theor. Phys. **116**, 1 (2006).
- [32] P. Descouvemont, E. C. Pinilla, and D. Baye, Prog. Theor. Phys. Suppl. **196**, 1 (2012).
- [33] J. Carlson and R. Schiavilla, Rev. Mod. Phys. **70**, 743 (1998).
- [34] A. Roggero, Phys. Rev. A **102**, 022409 (2020).
- [35] M. Rodríguez-Gallardo, J. M. Arias, J. Gómez-Camacho, A. M. Moro, I. J. Thompson, and J. A. Tostevin, Phys. Rev. C **72**, 024007 (2005).
- [36] E. C. Pinilla, D. Baye, P. Descouvemont, W. Horiuchi, and Y. Suzuki, Nucl. Phys. A **865**, 43 (2011).
- [37] J. Casal, J. Singh, L. Fortunato, W. Horiuchi, and A. Vitturi, Phys. Rev. C **102**, 064627 (2020).
- [38] W. R. Leo, *Techniques for Nuclear and Particle Physics Experiments: A How-to Approach* (Springer Berlin Heidelberg, 2012).
- [39] W. C. Haxton, K. M. Nollett, and K. M. Zurek, Phys. Rev. C **72**, 065501 (2005).
- [40] G. Orlandini and F. Turro, Few-Body Syst. **58** (2017).
- [41] V. Efros, W. Leidemann, and G. Orlandini, Nucl. Phys. A **631**, 658 (1998).
- [42] V. D. Efros, W. Leidemann, and V. Y. Shalamova, Few-Body Syst. **60** (2019).
- [43] Q. Chen, C. R. Howell, T. S. Carman, W. R. Gibbs, B. F. Gibson, A. Hussein, M. R. Kiser, G. Mertens, C. F. Moore, C. Morris, A. Obst, E. Pasyuk, C. D. Roper, F. Salinas, H. R. Setze, I. Slaus, S. Sterbenz, W. Tornow, R. L. Walter, C. R. Whiteley, and M. Whitton, Phys. Rev. C **77**, 054002 (2008).
- [44] R. Malone, A. Crowell, L. Cumberbatch, B. Fallin, F. Friesen, C. Howell, C. Malone, D. Ticehurst, W. Tornow, D. Markoff, B. Crowe, and H. Witała, Phys. Lett. B **835**, 137557 (2022).
- [45] R. A. Arndt, D. D. Long, and L. Roper, Nucl. Phys. A **209**, 429 (1973).
- [46] R. B. Wiringa, V. G. J. Stoks, and R. Schiavilla, Phys. Rev. C **51**, 38 (1995).
- [47] O. L. Ramírez Suárez and J.-M. Sparenberg, Phys. Rev. C **88**, 014601 (2013).
- [48] G. Lacroix, C. Semay, and F. Buisseret, Phys. Rev. E **86**, 026705 (2012).
- [49] H. Kanada, T. Kaneko, S. Nagata, and M. Nomoto, Prog. Theor. Phys. **61**, 1327 (1979).
- [50] M. Brodeur, T. Brunner, C. Champagne, S. Ethenauer, M. J. Smith, A. Lapierre, R. Ringle, V. L. Ryjkov, S. Bacca, P. Delheij, G. W. F. Drake, D. Lunney, A. Schwenk, and J. Dilling, Phys. Rev. Lett. **108**, 052504 (2012).
- [51] I. Sick, Phys. Rev. C **77**, 041302 (2008).
- [52] Y. Sun, T. Nakamura, Y. Kondo, Y. Satou, J. Lee, T. Matsumoto, K. Ogata, Y. Kikuchi, N. Aoi, Y. Ichikawa, K. Ieki, M. Ishihara, T. Kobayashi, T. Motobayashi, H. Otsu, H. Sakurai, T. Shimamura, S. Shimoura, T. Shinohara, T. Sugimoto, S. Takeuchi, Y. Togano, and K. Yoneda, Phys. Lett. B **814**, 136072 (2021).
- [53] A. Cobis, D. V. Fedorov, and A. S. Jensen, Phys. Rev. C **58**, 1403 (1998).
- [54] L. A. Souza, E. Garrido, and T. Frederico, Phys. Rev. C **94**, 064002 (2016).
- [55] J. Rotureau and U. van Kolck, Few-Body Syst. **54**, 725 (2012).
- [56] E. C. Pinilla, P. Descouvemont, and D. Baye, Phys. Rev. C **85**, 054610 (2012).